Optical Materials 58 (2016) 382–389

Contents lists available at ScienceDirect

Optical Materials

journal homepage: www.elsevier.com/locate/optmat

Achieving highly-enhanced UV photoluminescence and its origin in ZnO nanocrystalline films

Dinesh Thapa [a], Jesse Huso [a], John L. Morrison [b], Caleb D. Corolewski [c], Matthew D. McCluskey [c], Leah Bergman [a, *]

[a] Department of Physics, University of Idaho, Moscow, ID 83844, USA
[b] Division of Natural Sciences and Mathematics, Lewis-Clark State College, Lewiston, ID 83501, USA
[c] Department of Physics and Astronomy, Washington State University, Pullman, WA 99164, USA

ARTICLE INFO

Article history:
Received 27 March 2016
Received in revised form
22 April 2016
Accepted 5 May 2016
Available online 14 June 2016

Keywords:
ZnO
UV-photoluminescence
DC-sputtering
Raman
Native defects
Annealing

ABSTRACT

ZnO is an efficient luminescent material in the UV-range ~3.4 eV with a wide range of applications in optical technologies. Sputtering is a cost-effective and relatively straightforward growth technique for ZnO films; however, most as-grown films are observed to contain intrinsic defects which can significantly diminish the desirable UV-emission. In this research the defect dynamics and optical properties of ZnO sputtered films were studied via post-growth annealing in Ar or O_2 ambient, with X-ray diffraction (XRD), imaging, transmission and Urbach analysis, Raman scattering, and photoluminescence (PL). The imaging, XRD, Raman and Urbach analyses indicate significant improvement in crystal morphology and band-edge characteristics upon annealing, which is nearly independent of the annealing environment. The native defects specific to the as-grown films, which were analyzed via PL, are assigned to Zn_i related centers that luminesce at 2.8 eV. Their presence is attributed to the nature of the sputtering growth technique, which supports Zn-rich growth conditions. After annealing, in either environment the 2.8 eV center diminished accompanied by morphology improvement, and the desirable UV-PL significantly increased. The O_2 ambient was found to introduce nominal O_i centers while the Ar ambient was found to be the ideal environment for the enhancement of the UV-light emission: an enhancement of ~40 times was achieved. The increase in the UV-PL is attributed to the reduction of Zn_i-related defects, the presence of which in ZnO provides a competing route to the UV emission. Also, the effect of the annealing was to decrease the compressive stress in the films. Finally, the dominant UV-PL at the cold temperature regime is attributed to luminescent centers not associated with the usual excitons of ZnO, but rather to structural defects.

1. Introduction

ZnO is a II–VI semiconductor with a wide direct-bandgap in the UV-range ~3.37 eV and large exciton binding energy ~60 meV [1,2]. ZnO has garnered considerable attention due to its unique properties and wide range of applications in optoelectronic devices such as gas sensors [3–5], surface acoustic wave devices [6], transparent conductive contacts [7], solar cells [8,9], ultraviolet light-emitting diodes [10], and ultraviolet lasers [1,11]. Numerous methods have been reported for the growth of ZnO films such as molecular beam epitaxy [1], metal organic chemical vapor deposition [9], spray pyrolysis [3], pulsed laser deposition [8], and a magnetron sputtering technique [12]. In the present work, DC magnetron sputtering was utilized to grow ZnO films. This technique is considered to be relatively cost-effective and straightforward due to its simple setup. In order to realize the potential applications of ZnO films, it is crucial to achieve films with high-optical quality that exhibit a strong UV luminescence. However, most of the as-grown films, irrespective of the growth method or substrate, are commonly observed to contain some type of native defects [13] as well as structural defects. The presence of defects can lower the UV emission efficiency and create luminescent centers in the visible, thus limiting the applications of ZnO in optical device technologies. Previous studies have reported that post-growth annealing treatment is an effective approach to reduce the defect centers, resulting in the enhancement of the films' optical quality [12,14,15].

* Corresponding author.
E-mail address: Lbergman@uidaho.edu (L. Bergman).

http://dx.doi.org/10.1016/j.optmat.2016.05.008

In an effort to achieve an effective route towards enhancement of UV photoluminescence (PL), and gain further understanding of the defect dynamics involved in the process, this research focused on annealing studies and its impact on a wide range of the film's properties. Specifically, two as-grown films were subjected to annealing treatment under two different atmospheres: one film was annealed in an O_2 environment and the other in Ar. The scanning electron microscopy (SEM), X-ray diffraction (XRD), and Raman scattering studies indicate the significant improvement of crystal quality and stress relaxation upon annealing. Similarly, the band-edge properties that were investigated via absorption spectroscopy and Urbach analysis indicate that the band-edge characteristics of both annealed films exhibit improvement relative to the as-grown film. The native defects specific to our films were also analyzed via luminescence spectroscopy. It was found that the as-grown ZnO film is rich in Zn_i that were annealed out under either Ar or O_2 ambient. The O_2 environment was found to introduce some O_i optical centers, while the Ar annealing ambient was found to be the ideal environment for the enhancement of the UV-light emission. The above results are discussed below in terms of the stabilities of the native defects in ZnO with respect to the sputtering growth technique and annealing environments. Finally, the UV-PL at the cold temperature regime was attributed to luminescent centers not associated with the usual excitons of ZnO but rather to structural defects. At room temperature the two emissions convolve.

2. Experiment

ZnO films were grown on (0001) sapphire substrates using a DC magnetron sputtering system. The sputtering chamber was evacuated to the base pressure of 10^{-6} Torr, and deposition of the films was carried out by sputtering the Zn metal target in an oxygen-argon gas mixture at a pressure of 11 mTorr and a delivered power of 30 W. Two films were grown for an hour at 250 °C. In order to examine the effect of post-annealing treatment on the optical and structural properties of the as-grown films, the films were annealed at 900 °C (1173 K) for 1 h each under a different atmosphere of ultra-high purity O_2 and Ar gases using a Lindberg/Blue M quartz tube furnace controlled by a Yokogawa UP-150 temperature controller. The as-grown sample was placed in a cleaned alumina boat and was inserted into the quartz tube. The inlet and the outlet gas flexible tubes were connected via compression fittings. For Ar annealing, initially the gas lines were purged for 10 min, setting the Ar flow-rate at 1255 cm^3/min. Then, the Ar flow rate was reduced to 273 cm^3/min and the annealing process was started. A similar process was performed for O_2 with flow rates of 100 cm^3/min for purging, and 50 cm^3/min during annealing. The relatively lower O_2 flow rate during the annealing was chosen in consideration of its reactive nature. The purging was done at room-temperature. For the annealing, the program of the furnace was set with a ramp-up and rump-down time of 30 min. The gas flow was continued during the cooling process.

Annealing at such high temperatures can result in improvement in the crystal structure, while annealing under a different atmosphere can reveal the nature of defects existing in the films. Utilizing a well-known optical interference technique [16], the thickness of the films was found to be ~500–600 nm. Transmission measurements were performed on the films using an Agilent 300 Cary UV–Vis transmission system in double beam mode. The photoluminescence experiments were carried out using a JY-Horiba Fluorolog-3 spectrometer with an excitation source of an Xe lamp. To investigate the origin of the UV PL, the cold temperature PL measurements were performed utilizing a Jobin-Yvon T6400 micro Raman and PL system in conjunction with an Instec 621 V microcell customized for UV measurements. Structural properties of the films were determined by XRD using a Siemens Diffractometer D5000 with the Cu Kα1 line operating in 2 theta mode. The surface morphology of the films was examined utilizing SEM.

3. Results and discussion

3.1. Structural, transmission, and Urbach energy studies

Fig. 1(a, b, c) presents the SEM images of both the as-grown and annealed films. Under high magnification, the image of the as-grown ZnO film reveals that the film consists of a granular morphology with significant secondary nucleation (Fig. 1(a)). In contrast, in both annealed films the grains are well defined and exhibit a much improved morphology. No significant difference between the two annealed films is evident from the SEM images. In order to gain further knowledge on the structural properties of the films, XRD studies were conducted. The XRD scans were referenced to the (0002) line of the sapphire substrate. As can be seen in Fig. 2, the XRD patterns of the as-grown and both of the O_2 and Ar

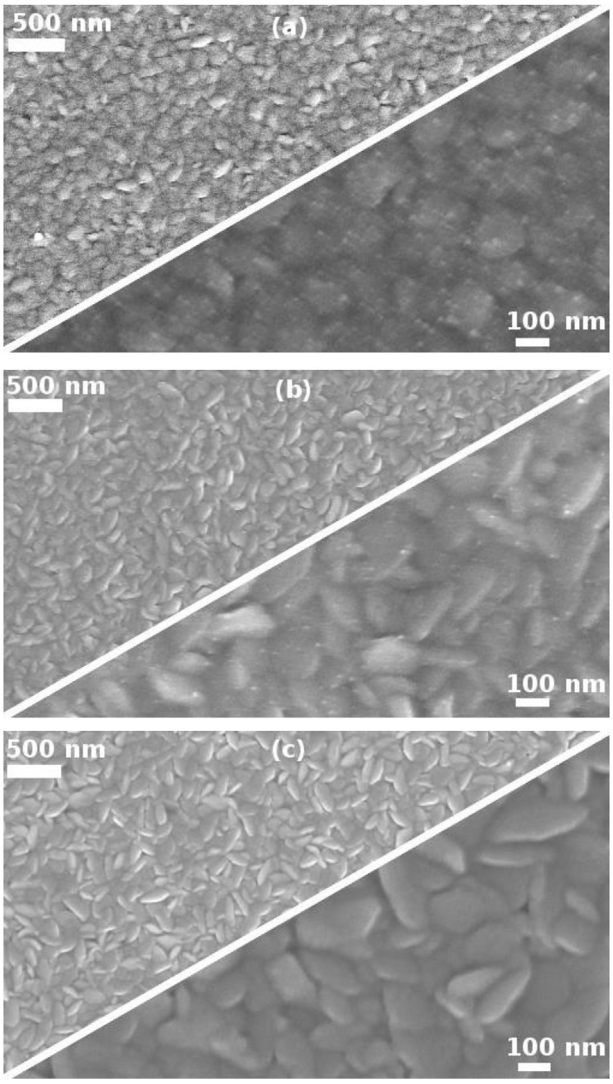

Fig. 1. SEM image of ZnO films: (a) as-grown, (b) O_2 annealed, and (c) Ar annealed, under low and high magnifications showing their surface morphology.

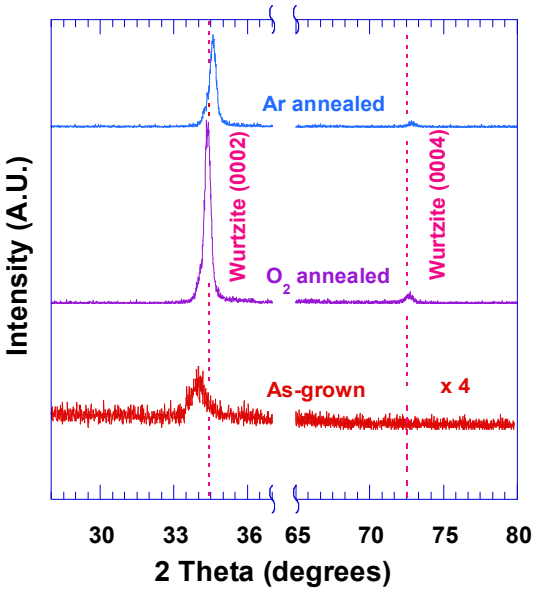

Fig. 2. XRD diffraction patterns of ZnO films: as-grown, O_2 annealed, and Ar annealed. An additional wurtzite (0004) peak in the annealed films is visible.

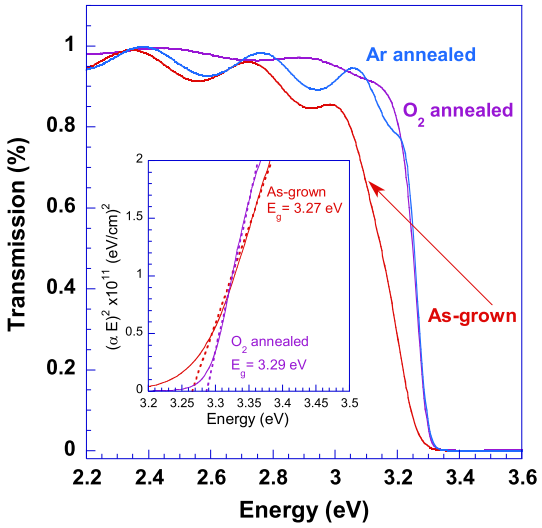

Fig. 3. Transmission spectra of ZnO films: as grown and annealed. The sinusoidal features at low energies are due to the thin film interference. The inset is the Tauc plot for the determination of the bandgap of the films: ~3.27 eV for the as-grown, ~3.29 eV for the O_2 annealed. That of the Ar annealed (not shown) is the same as the O_2 sample.

annealed ZnO films showed the (0002) wurtzite peak, indicating that the films are preferentially oriented along the c-axis. The presence of an additional weak diffraction peak, corresponding to (0004) wurtzite structure, in both annealed films indicates their improved crystallinity. Moreover, the (0002) diffraction peak shows strong enhancement in intensity in both annealed films compared to that of the as-grown film. The full-width at half-maximum (FWHM) value of the (0002) diffraction peak was found to be ~0.80° for the as grown sample, and much smaller for both of the annealed ones: ~0.30°.

The average grain size was calculated using Scherrer's formula with the calculated FWHM listed above. The calculation indicates that the average grain size for the as-grown sample is ~11 nm, while it is ~31 nm for both of the annealed samples. It is notable that these calculated values of the grain size are relatively smaller than those presented in the SEM images. A similar observation has been reported previously where the grain sizes calculated using XRD measurements was found to be smaller than the values revealed under SEM [17,18]. The underlying reasons for the smaller values of grain size estimated via XRD have been attributed to the presence of defects, and to the nature of the method itself [17,18]. Specifically, the XRD method provides preferential information about the size of the region with highly-coherent scattering; such scattering usually occurs in smaller regions [19].

Informative methods that may provide additional insight into crystal dynamics and material's quality are transmission and absorption spectroscopies. One aspect of absorption analysis is what is known as Urbach energy [20,21] that yields a measure of a semiconductor's defects and imperfection, as is discussed in the following paragraphs.

The transmission spectra acquired for the as-grown and annealed ZnO films are shown in Fig. 3. As can be seen in the figure, the spectra of both annealed samples exhibit a sharper absorption edge relative to that of the as-grown film. Furthermore, no obvious difference can be observed between the transmission spectra characteristics of the films annealed under either Ar or O_2 ambient.

Typically, the presence of defects that include impurities and structural disorders in a semiconductor are known to produce the localized energy states (band tail) within the bandgap, and a good measure of the extent of these states may be given by the Urbach energy [20,21]. The Urbach energy, E_U, can be ascertained using the well-known Urbach model [20–23]. According to the model, the absorption coefficient below the optical bandgap follows exponential dependence with the photon energy, i.e., $\alpha(E) = Ce^{E/E_U}$, where $\alpha(E)$ is the absorption coefficient as a function of energy, and C is a constant. Fig. 4 presents the Urbach energy analysis for all of the samples, which yields E_U values of 85, 36, and 34 meV for the as-grown, O_2, and Ar annealed films, respectively. The significant reduction in the Urbach energy for both annealed films indicates that lower concentration of defects exists in these samples relative to that of as-grown film. As in the case of the XRD analysis, the

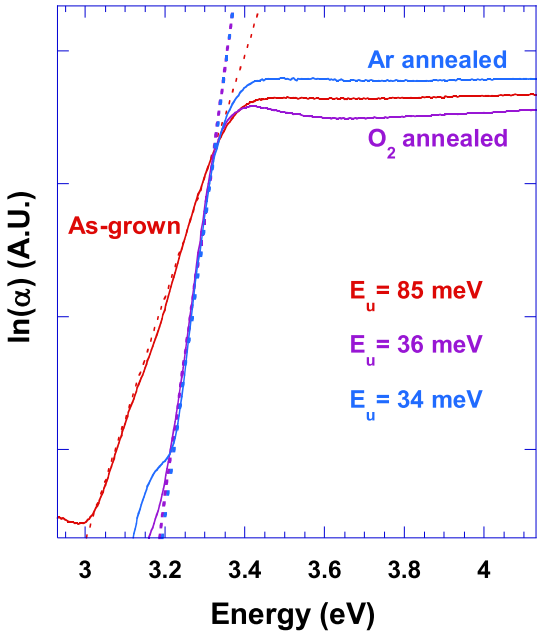

Fig. 4. Urbach analysis for the ZnO films. Urbach energy (E_u) has been determined via fitting of the Urbach model in the linear region below the bandgap. E_u = 85 meV for the as-grown film, and 36 and 34 meV for the O_2 and Ar annealed films, respectively.

similar values of Urbach energy of both annealed samples imply that both annealing environments are very useful for defect reduction in ZnO films.

Further studies on the nature of the defects, their dynamics in the annealing process, and their relation to enhancement of the UV-PL, is presented in following section.

3.2. Photoluminescence study

3.2.1. As-grown ZnO film

The above studies indicate that both annealing processes resulted in improving the film quality. However, these studies did not convey insight into the issue of native defects prevalent to ZnO. It has been established that native defects in ZnO luminesce in the visible range, and that PL is a quite informative approach regarding the identification of these defects. In most studies of ZnO, PL spectra show two emission bands [13,14,24–26]. One of these bands, the near band edge (NBE) emission, is located near the bandgap and lies in the ultraviolet region. Another band is located in the visible spectral region and is generally known as the deep level emission (DLE) [8,24,27,28]. The NBE emission peak is typically attributed to excitonic recombination, while the origin of the DLE band is usually attributed to optical centers associated with impurities such as native defects. Since the energetics of the NBE and DLE can provide two competing routes to carrier recombination, it is usually desirable to minimize the defect centers in order to enable the enhancement of the UV emission [28]. In the following, we present a study whereby the presence of native impurities was minimized during annealing, and efficient UV emission is achieved.

As can be seen in Fig. 5(a), PL spectra of the as-grown films showed a weak and broad PL peak extending from the visible to the UV region. The deconvolution of the spectral-line indicates that a visible emission is centered at ~2.80 eV, and the UV emission is at ~3.25 eV. The UV PL is attributed to the band-edge emission in ZnO, and its origin in our sample will be discussed in further detail in a later section. Hereafter, the emission peak at ~2.80 eV will be referred to as the blue emission. As can be seen in Fig. 5(a), the UV-PL intensity is relatively weak compared to the blue emission.

The observed blue emission has been reported previously in ZnO films [29], micro whiskers [30], and nanoparticles [31]. Fang et al. have previously investigated the blue emission, ~2.9 eV, of the sputtered ZnO films via PL and electrical measurements, and found it to be correlated with the density of Zn_i defects in the films [29]. Xu et al. studied, via XRD, EDS (energy dispersive X-ray spectroscopy), and EPR (electron paramagnetic resonance), the evolution of blue (~2.95 and 2.83 eV) and green emissions (~2.44 eV) of ZnO micro whiskers grown by a vapor-phase transport method [30]. They found a correlation between the evolution these visible emissions with structural features, stoichiometry, and paramagnetic defect centers. The blue and green emissions in Xu's study were suggested to be related to Zn_i and V_O^+, respectively, formed during growth [30]. Additionally, Zeng et al. have established that blue luminescence (~2.8–3.0 eV) in the ZnO nanoparticles increased rapidly under low annealing temperature, and quenched under high annealing temperature in air and N_2 atmosphere [31]. In their study, the emission was discussed in terms of transition from Zn_i-related defect levels to the valence band. Kayaci et al. have confirmed the existence of Zn_i related defects in ZnO nano-structures via X-ray photoelectron spectroscopy (XPS), and attributed the blue PL (2.83–3.10 eV) to these defects [32]. Table I presents some of the properties relevant to this paper of the native defects in ZnO [29–43].

Fig. 6 presents a tentative energy level diagram for Zn_i related defects in ZnO which is consistent with the blue emission observed in this study. The bandgap value of our ZnO film was determined via Tauc analysis to be ~3.27 eV (see inset to Fig. 3). Taking this value into account in conjunction with the PL value of 2.80 eV, the Zn_i-

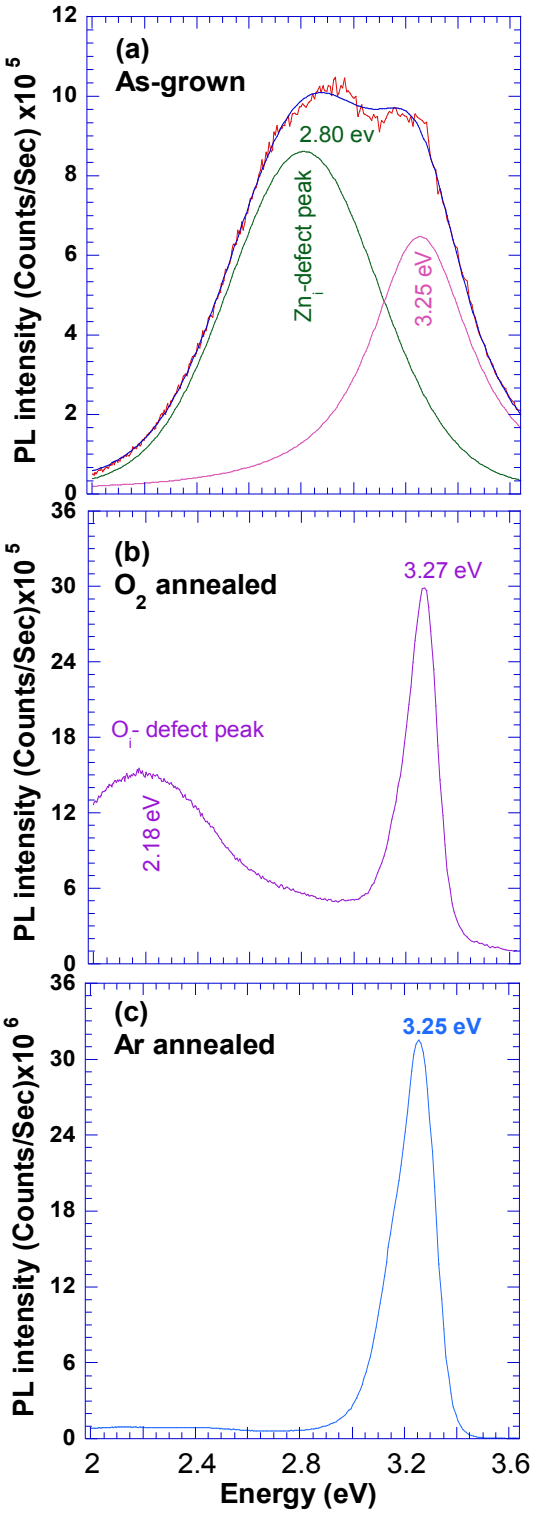

Fig. 5. Room temperature PL spectra of the ZnO films: (a) PL of the as-grown film, showing two peaks at ~2.80 and 3.25 eV that were obtained via a Voigt profile fitting to the experimental spectrum, (b) The spectrum of the O_2 annealed film showing an enhanced UV-PL peak at 3.27 eV and an O_i related peak at 2.18 eV, and (c) PL of the Ar annealed film exhibiting the enhanced UV-PL at 3.25 eV with a nearly quenched visible emission peak. The UV-PL intensity of the Ar annealed film is about 40 times stronger compared to that of the as-grown film.

Table 1
Defect energy levels of Zn_i and O_i native defects and ascribed PL emission and migration barrier corresponding to these defects.

Defect	PL emission	Energy Levels (values in eV)	Mobility temp (migration barrier)
Zn_i	Blue	~0.4 eV below CB [34]	170 K [37]
or	~2.9 eV [29]	~0.30 eV below CB [33]	(0.57 eV) [38]
$Zn_{i\ -related}$	(~2.83 and 2.95 eV) [30]	~0.28 eV below CB [35]	
	~2.8–3.0 eV [31]	0.15 eV below CBM (+2/+1) [36]	
	~2.83–3.10 eV [32]		
	~2.88 eV [33]		
O_i	Yellow	1.18 eV above VBM (-/2-) [41]	440 K [38,43]
	~2.11 eV [39]	1.59 eV above VBM (-/2-) [38]	(1.1 eV) [38]
	~2.13 eV [40]	~1.09 eV above the VB [35,42]	

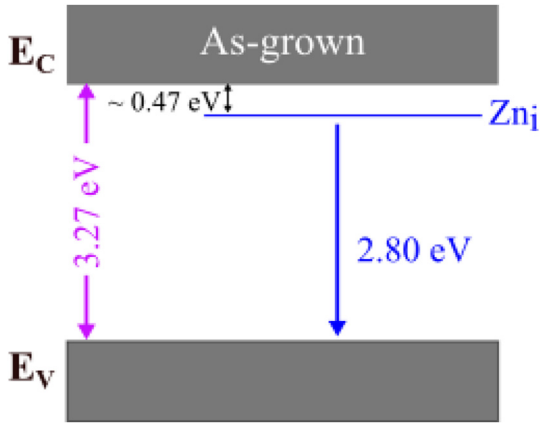

Fig. 6. Schematic energy band-diagram of the proposed transition mechanisms for the as-grown ZnO film. The bandgap value, 3.27 eV, was obtained via the Tauc plot analysis (see the inset to Fig. 3). The blue PL at 2.80 eV is assigned to a transition from a Zn_i-related defect level at ~0.47 eV to the valence band.

related defect level appears to lie ~0.47 eV below the conduction band. This value for the Zn_i energy level is in good agreement, up to experimental error, with the values summarized in Table I.

In typical cases, the formation energy of Zn_i is reported to be quite high, but can be reduced in Zn-rich growth conditions [31,36,44]. For the study presented here, a DC sputtering technique was utilized to grow the films, which can lead to the growth of Zn-rich films, thereby favoring the formation of Zn_i-related defects in the films. The phenomenon of sputtering growth which results in Zn-rich films is commonly reported in the literature [12,19,45] and can be understood by noting that sputtering involves the competing processes of target oxidation and removal of target material. To achieve growth, the target material, i.e., Zn, must be removed at a sufficient rate so as to prevent an oxide overcoating of the target. However, by removing the target material at high rates, the sputtered material may not be completely oxidized, a condition that favors Zn-rich film. In principle, Zn-rich films may contain Zn_i as well as oxygen vacancies (V_O) as native defects. The PL of V_O was suggested to be in the green spectral-range of ~2.53–2.34 eV [8], and as can be seen in Fig. 5(a), it is not pronounced in our PL spectrum. The latter imply that V_O is not a dominant native impurity in the as-grown ZnO film. It bears noting that the stability of Zn_i is still an ongoing research topic; however, several experimental results showed convincing evidence that Zn_i and related defects centers can be present in the ZnO sample [30–32].

3.2.2. Annealed ZnO films

Having examined the as-grown film, we now turn our attention to the ZnO film annealed at 900 °C under oxygen atmosphere. As can be seen in Fig. 5(b), the O_2 annealed films showed a much more pronounced UV emission than that of the as-grown film. Additionally, the blue PL that was observed in the as-grown film at ~2.80 eV is not detectable, and a new visible PL ~2.18 eV with relatively weak intensity is observed. The disappearance of blue emission, due to Zn_i-related defects, after O_2 annealing treatment can be understood in terms of the fast diffusive nature of Zn_i-related defects. From density-functional calculations, Janotti et al. reported the migration barrier of Zn_i to be 0.57 eV, which is considered to be relatively low [38]. Alternatively, the mobility temperature of these defects, which was previously found to be ~170 K (see Table I), is much lower than our annealing temperature 1173 K. In light of these properties, it is reasonable to expect that Zn_i related defects should diffuse out or incorporate into substitution lattice sites.

The emergence of the visible emission PL ~2.18 eV, also known as the yellow luminescence [39,40,46,47], has been previously studied by several groups, and was attributed to oxygen interstitial (O_i) defects in ZnO [39,40,46]. We surmise that annealing under O_2 ambient is conducive to the formation of O_i defects. The high partial pressure of oxygen in the environment will lead to diffusion of oxygen into the lattice, resulting in O_i defects. While the formation energy of O_i defects is predicted to be high in ZnO [41], resulting in an expectation of minimal O_i defect concentration, O_i defects are also mobile above 440 K [38,43] (see Table I). Thus the combination of high annealing temperature (1173 K) and high oxygen partial pressure creates conditions favorable for the formation of O_i defects, and also to rapid diffusion through the lattice. With regards to the bandgap mapping for this sample, theoretical calculation by Janotti et al. has previously predicted that O_i defects form a deep acceptor level at 1.18 eV above the valence band [41]. The bandgap of the O_2 annealed ZnO film, as was determined from Tauc analysis, is ~3.29 eV, while the PL is at 2.18 eV: these energetics agree with a transition from the conduction band to a state at ~1.11 eV above the valence band. Our obtained experimental value agrees closely with the theoretical value of 1.18 eV reported by Janotti et al. [41].

As is shown in Fig. 5(c), the UV PL for the Ar annealed ZnO film is significantly enhanced, while there is only a trace of the visible emission. This can be understood by noting that during annealing under Ar atmosphere the Zn_i-related defects residing in the as-grown film will be eliminated. This dynamic is similar to that discussed for the case of the O_2 annealed sample: the low mobility temperature and low migration barrier of the Zn_i-related defects will cause out-diffusion or lattice incorporation of these defects. Additionally, Ar is a non-reactive atmosphere, and thus no new defects should be introduced. The key point is that the UV PL intensity of the Ar annealed film is about 40 times stronger compared to that of the as-grown film. The enhancement of the UV luminescence is attributed to the elimination of the competing routes to the UV light emission due to defects.

3.3. Raman study

As can be seen in the SEM images, the morphology of both annealed samples was significantly improved relative to that of the as-grown sample. Also it is expected that annealing will relax the stress state of a sample. In general, Raman scattering was proven to be a highly sensitive spectroscopy, enabling the assessment of a material's internal stress via the frequency shift of a particular Raman mode. In the following we present Raman analysis of the three ZnO samples. The Raman spectra were acquired in a back scattering geometry utilizing the 325 nm (3.81 eV) HeCd laser line. The experimental error is ~± 1 cm^{-1}. Since that excitation energy is close to the bandgap of ZnO, resonant Raman scattering occurs resulting in enhanced LO mode [48]. Fig. 7 presents the Raman spectra of the films. As can be seen in the figure, the LO-mode exhibits a systematic shift towards the lower frequency, starting at 578 cm^{-1} for the as-grown sample, then 575 cm^{-1} for the oxygen annealed, and 573 cm^{-1} for the argon annealed sample; i.e., a total shift of ~5 cm^{-1}. The shift towards the lower frequency may be suggestive of a relaxation of intrinsic compressive stress. The pressure coefficient $(\partial\omega/\partial P)$ for the LO-mode in ZnO (where ω is the phonon frequency) was found previously to be in the range of ~4.14–4.56 cm^{-1}/GPa [49,50]; a similar pressure coefficient, ~4.9 cm^{-1}/GPa, was obtained by our group for the case of ZnO doped with a small percentage of Mg [51]. Since the observed Raman shift is ~5 cm^{-1}, a relaxation of ~1 GPa took place upon annealing. Furthermore, this relaxed stress of ~1 GPa is comparable to those obtained previously via XRD and curvature measurement studies of ZnO thin films grown via the sputtering method [52,53]. The compressive stress in our samples can be attributed to structural defects and Zn aggregation, both of which were significantly reduced during the annealing process. In addition, the Raman linewidth of the films shows narrowing upon annealing, as is indicated in Fig. 7. The narrowing may be attributed to the increase in the phonon lifetime, which is a result of the improved crystallinity of both annealed films.

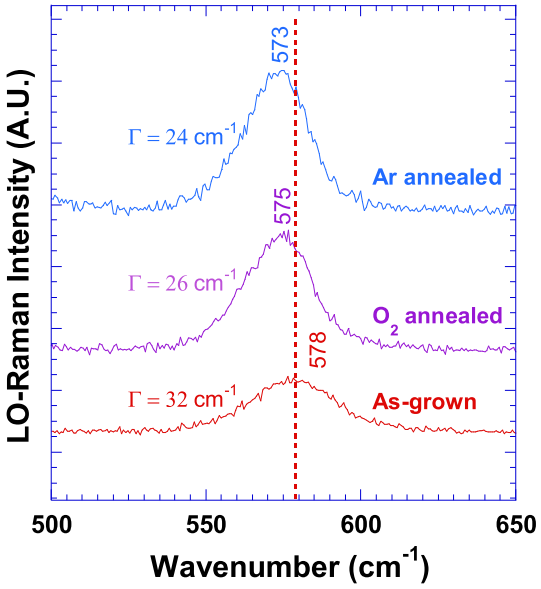

Fig. 7. The LO-Raman mode spectra of the ZnO films. The LO mode of O_2 and Ar annealed films show a red-shift of 3 and 5 cm^{-1}, respectively, relative to the as-grown film, attributed to stress relaxation. Smaller Raman linewidths of the annealed films indicate their improved crystallinity.

3.4. Origin of UV PL

Having found that Ar annealing generates the highest UV emission intensity, we next investigate its actual origin. Fig. 8 presents the PL spectra at 77 K for the Ar annealed ZnO film along with that of ZnO nanocrystals reported in our previous work [54]. Additionally, the cold temperature PL spectra of ZnO single crystal is also included as a reference. As can be seen in Fig. 8, the PL spectra of the single crystal ZnO consists of two main spectral lines at 3.362 and 3.376 eV. These two PL emissions have been extensively studied by various groups, and have been assigned to a neutral donor-bound exciton D^oX and the *A*-exciton *X*, respectively [54,55]. As is shown in Fig. 8, in the spectrum of the Ar annealed sample, the D^oX and the *A*-exciton are present at nearly the same energies as those of the single crystal. A key finding is that in addition to two excitonic emission lines, the PL of ZnO film exhibits a strong line at ~3.314 eV, referred to as the ε-PL, which is red shifted by ~58 meV from the *A*-exciton. The ε-emission was previously found by us to be the dominant PL in ZnO nanocrystals of size ~40 nm, and was attributed to structural defects [54]. The ZnO nanocrystals were grown via a chemical approach, while the films were deposited via a sputtering technique; both methods resulted in a nano-scale granular morphology which seems to be the reason for the onset of the specific UV luminescence. Furthermore, as can be seen in Fig. 8, at room temperature the band-edge PL of the film becomes a convolution of the ε-PL with that of the exciton peaks.

A discussion follows concerning the impact of the choice of substrates on the optical properties. The research of our group focuses on semiconductors with extreme bandgaps that include ZnO-based alloys such as $Mg_xZn_{1-x}O$. The bandgaps of these alloys span a large UV range of ~3.3 eV–~6 eV [20]. In order to ensure the

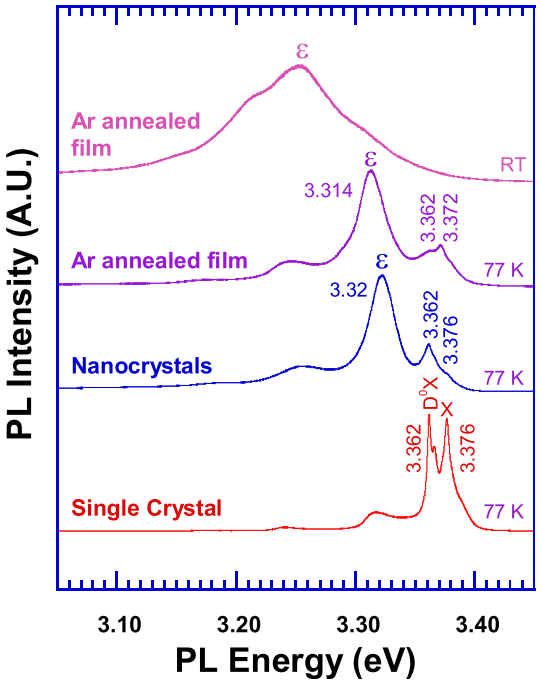

Fig. 8. The PL spectra at 77 K of ZnO samples (lower three traces): single crystal, nanocrystals, and Ar annealed film. The single crystal spectrum exhibits the usual ZnO excitons: the bound exciton D^oX ~3.362 eV, and the free A-exciton X ~3.376 eV. The peaks observed for the Ar annealed film exhibit the ZnO excitons and an additional peak, ε -PL, related to structural defects. The nanocrystals have a similar PL spectrum to that of the film. The upper spectrum was acquired at room temperature from the Ar-annealed film. The phonon replicas are at the lower energy range. The spectrum for the nanocrystals is from Ref. [54].

transparency of the film/substrate product, as is desirable for some technological applications, substrates with a wide-bandgap are chosen. In this research, two-side polished c-face sapphire substrates were used. The bandgap of a single-crystal sapphire is ~8.8 eV [56] which makes it optically compatible to the $Mg_xZn_{1-x}O$ films. The other substrate that we commonly use, due to its UV compatibility, is quartz with a reported bandgap ~8.9 eV [57].

Our ongoing research did not find a significant differences among the optical properties of the films using either sapphire or quartz as a substrate. Fig. 9 presents the PL spectra of as-grown ZnO film and that of the Ar annealed film grown on quartz. As can be seen in the figure, the PL characteristics of the as-grown film and that of the Ar annealed are very similar to those of the ZnO grown on sapphire substrate (see Fig. 5(a), (c); an enhancement, of ~35-times, for the UV emission was achieved. Future research will address additional substrates of relevance to opto-electronic technologies, such as silicon and GaN.

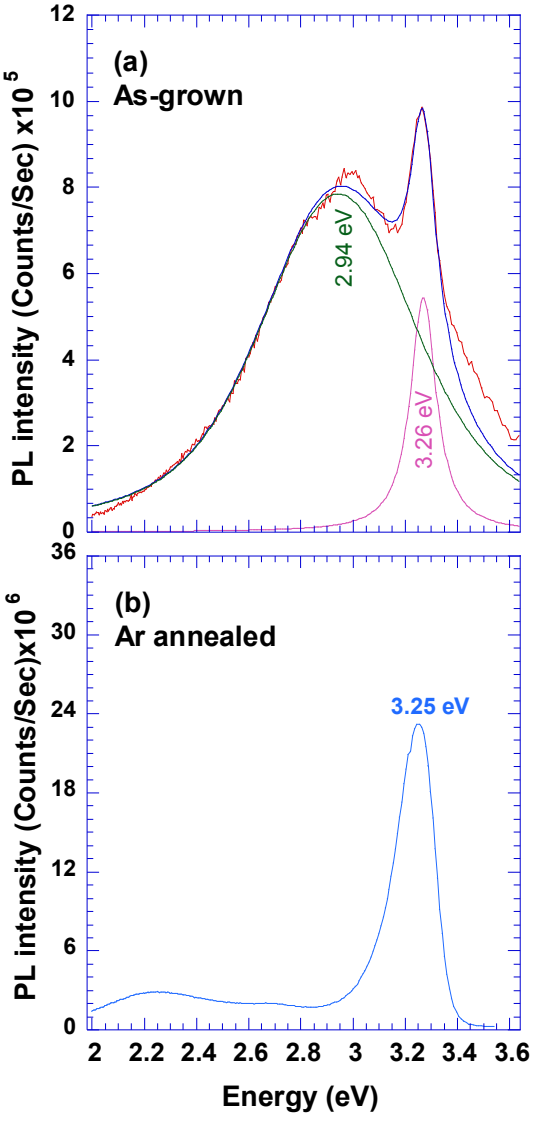

Fig. 9. The PL spectra of the ZnO film grown on quartz substrate. The as grown film (a), and (b) the Ar annealed film.

4. Conclusions

In this study we investigated the effect of post growth annealing under Ar and O_2 environments on the properties of ZnO films with the objective of achieving high intensity UV photoluminescence. The SEM and the XRD studies both indicate the improvement of crystal morphology upon annealing with no significant dependence on the annealing environment. Moreover, the band-edge properties that were investigated via absorption spectroscopy and Urbach analysis indicate that the band-edge characteristics of both annealed films exhibit significant improvement relative to the as-grown film. However, similar to the XRD and SEM studies, no obvious difference was evident between the band-edge characteristics of the films annealed under either Ar or O_2 ambient. Similarly, the Raman linewidth of both annealed samples, having an approximate value which is smaller than that of the as-grown sample, point to a similar extent of improvement of the crystal structure in either annealing environment. The Raman frequency shift is indicative of stress relaxation of ~1 GPa in the annealed samples.

The native defects specific to our films were analyzed via luminescence spectroscopy. It was found that the as-grown ZnO film exhibits relatively low UV-PL intensity ~3.25 eV, and an additional pronounced visible PL at ~2.80 eV attributed to Zn_i related defects. The presence of these defects in the films was attributed to the nature of the sputtering growth technique which supports Zn-rich growth conditions. After annealing the samples in either Ar or O_2 ambient, the 2.8 eV center diminished and the desirable UV-PL was significantly increased. The Ar annealing ambient was found to be the ideal environment for the enhancement of the UV-light emission: an enhancement of ~40 times was achieved. The increase in the UV-PL is attributed to the reduction of Zn_i-related defects, the presence of which in ZnO provides a competing route to the UV light transition. Moreover, the above results were discussed in terms of the stability of the native defects in ZnO with respect to the sputtering growth technique and annealing environments.

As was mentioned above, the annealing treatments under either O_2 or Ar diminished the inherent Zn_i related defects and improved the morphology of the films. The O_2 environment, in addition, introduced a nominal concentration of O_i defects, as can be inferred from its relative weak PL. As indicated by Urbach energies, XRD, and Raman linewidths that were for most part invariant for both annealing environments, the O_i concentration did not have a significant impact on crystal quality. The O_i centers, however, may act as a competing mechanism to the UV-PL. The energy band diagram and mapping for the as-grown and oxygen annealed samples that were ascertained via PL and Tauc plots were found to be consistent with theoretical predictions and previous experimental studies for the energy levels of Zn_i and O_i native defects.

Finally, the UV-PL at the cold temperature regime was attributed to luminescent centers not associated with the usual excitons of ZnO, but rather to structural defects. At room temperature the two emissions convolve.

Acknowledgments

The authors gratefully acknowledge the U.S. Department of Energy, Office of Basic Energy Science, Division of Materials Science and Engineering under grant No. DE-FG02-07ER46386.

References

[1] Z.K. Tang, G.K.L. Wong, P. Yu, M. Kawasaki, A. Ohtomo, H. Koinuma, Y. Segawa, Appl. Phys. Lett. 72 (1998) 3270.

[2] V.V. Ursaki, I.M. Tiginyanu, V.V. Zalamai, V.M. Masalov, E.N. Samarov, G.A. Emelchenko, F. Briones, J. Appl. Phys. 96 (2004) 1001–1006.
[3] S.A. Studenikin, M. Cocivera, W. Kellner, H. Pascher, J. Lumin. 91 (2000) 223–232.
[4] N.J. Dayan, S.R. Sainkar, R.N. Karekar, R.C. Aiyer, Thin Solid Films 325 (1998) 254–258.
[5] B.B. Rao, Mater. Chem. Phys. 64 (2000) 62–65.
[6] C.R. Gorla, N.W. Emanetoglu, S. Liang, W.E. Mayo, Y. Lu, M. Wraback, H. Shen, J. Appl. Phys. 85 (1999) 2595–2602.
[7] K.L. Chopra, S. Major, D.K. Pandya, Thin Solid Films 102 (1983) 1–46.
[8] H.S. Kang, J.S. Kang, J.W. Kim, S.Y. Lee, J. Appl. Phys. 95 (2004) 1246–1250.
[9] W.W. Wenas, A. Yamada, K. Takahashi, M. Yoshino, M. Konagai, J. Appl. Phys. 70 (1991) 7119.
[10] H. Ohta, K. Kawamura, M. Orita, M. Hirano, N. Sarukura, H. Hosono, Appl. Phys. Lett. 77 (2000) 475–477.
[11] D.C. Reynolds, D.C. Look, B. Jogai, Solid State Commun. 99 (1996) 873–875.
[12] W.S. Shi, O. Agyeman, C.N. Xu, J. Appl. Phys. 91 (2002) 5640.
[13] F.K. Shan, G.X. Liu, W.J. Lee, B.C. Shin, J. Appl. Phys. 101 (2007) 053106.
[14] Y.R. Jang, K.-H. Yoo, S.M. Park, J. Vac. Sci. Technol. A 28 (2010) 216–219.
[15] L.M. Kukreja, P. Misra, J. Fallert, D.M. Phase, H. Kalt, J. Appl. Phys. 112 (2012) 013525.
[16] J.C. Manifacier, J. Gasiot, J.P. Fillard, J. Phys. [E] 9 (1976) 1002.
[17] J. Huso, J.L. Morrison, H. Che, J.P. Sundararajan, W.J. Yeh, D. Mcllroy, T.J. Williams, L. Bergman, J. Nanomater. 2011 (2011) 1–7.
[18] K. Srinivasarao, G. Srinivasarao, K.V. Madhuri, K. Krishna Murthy, P.K. Mukhopadhyay, Indian J. Mater. Sci. 2013 (2013) 1–7.
[19] V.V. Khomyak, M.M. Slyotov, I.I. Shtepliuk, G.V. Lashkarev, O.M. Slyotov, P.D. Marianchuk, V.V. Kosolovskiy, J. Phys. Chem. Solids 74 (2013) 291–297.
[20] J. Huso, H. Che, D. Thapa, A. Canul, M.D. McCluskey, L. Bergman, J. Appl. Phys. 117 (2015) 125702.
[21] M.F. Malek, M.H. Mamat, Z. Khusaimi, M.Z. Sahdan, M.Z. Musa, A.R. Zainun, A.B. Suriani, N.D. Md Sin, S.B. Abd Hamid, M. Rusop, J. Alloys Compd. 582 (2014) 12–21.
[22] S. Dutta, S. Chattopadhyay, D. Jana, A. Banerjee, S. Manik, S.K. Pradhan, M. Sutradhar, A. Sarkar, J. Appl. Phys. 100 (2006) 114328.
[23] J.I. Pankove, Optical Processes in Semiconductors, Dover, New York, 1975.
[24] M. Willander, O. Nur, J.R. Sadaf, M.I. Qadir, S. Zaman, A. Zainelabdin, N. Bano, I. Hussain, Materials 3 (2010) 2643–2667.
[25] L. Irimpan, D. Ambika, V. Kumar, V.P.N. Nampoori, P. Radhakrishnan, J. Appl. Phys. 104 (2008) 033118.
[26] D. Li, Y.H. Leung, A.B. Djurišić, Z.T. Liu, M.H. Xie, S.L. Shi, S.J. Xu, W.K. Chan, Appl. Phys. Lett. 85 (2004) 1601.
[27] C. Tsakonas, W. Cranton, F. Li, K. Abusabee, A. Flewitt, D. Koutsogeorgis, R. Ranson, J. Phys. D Appl. Phys. 46 (2013) 095305.
[28] Y.G. Wang, S.P. Lau, X.H. Zhang, H.H. Hng, H.W. Lee, S.F. Yu, B.K. Tay, J. Cryst. Growth 259 (2003) 335–342.
[29] Z. Fang, Y. Wang, D. Xu, Y. Tan, X. Liu, Opt. Mater. 26 (2004) 239–242.
[30] X. Xu, C. Xu, J. Dai, J. Pan, J. Hu, J. Phys. Chem. Solids 73 (2012) 858–862.
[31] H. Zeng, G. Duan, Y. Li, S. Yang, X. Xu, W. Cai, Adv. Funct. Mater. 20 (2010) 561–572.
[32] F. Kayaci, S. Vempati, I. Donmez, N. Biyikli, T. Uyar, Nanoscale 6 (2014) 10224–10234.
[33] N.S. Han, H.S. Shim, J.H. Seo, S.Y. Kim, S.M. Park, J.K. Song, J. Appl. Phys. 107 (2010) 084306.
[34] B. Lin, Z. Fu, Y. Jia, Appl. Phys. Lett. 79 (2001) 943–945.
[35] S. Kuriakose, B. Satpati, S. Mohapatra, Phys. Chem. Chem. Phys. 16 (2014) 12741–12749.
[36] P. Erhart, K. Albe, A. Klein, Phys. Rev. B 73 (2006) 205203–205211.
[37] M.D. McCluskey, S.J. Jokela, J. Appl. Phys. 106 (2009) 071101.
[38] A. Janotti, C.G. Van de Walle, Rep. Prog. Phys. 72 (2009) 126501.
[39] X.L. Wu, G.G. Siu, C.L. Fu, H.C. Ong, Appl. Phys. Lett. 78 (2001) 2285–2287.
[40] C. Chandrinou, N. Boukos, C. Stogios, A. Travlos, Microelectron. J. 40 (2009) 296–298.
[41] A. Janotti, C.G. Van de Walle, J. Cryst. Growth 287 (2006) 58–65.
[42] C.H. Ahn, Y.Y. Kim, D.C. Kim, S.K. Mohanta, H.K. Cho, J. Appl. Phys. 105 (2009) 013502.
[43] A. Janotti, C.G. Van de Walle, Phys. Rev. B 76 (2007) 165202.
[44] A.F. Kohan, G. Ceder, D. Morgan, C.G. Van de Walle, Phys. Rev. B 61 (2000) 15019–15027.
[45] S.-Y. Chu, W. Water, J.-T. Liaw, J. Eur. Ceram. Soc. 23 (2003) 1593–1598.
[46] L.E. Greene, M. Law, J. Goldberger, F. Kim, J.C. Johnson, Y. Zhang, R.J. Saykally, P. Yang, Angew. Chem. Int. Ed. 42 (2003) 3031–3034.
[47] M.A. Reshchikov, J. Garbus, G. Lopez, M. Ruchala, B. Nemeth, J. Nause, Mater. Res. Soc. Symp. Proc. 957 (2007) 219–224.
[48] L. Bergman, X.-B. Chen, J. Huso, J.L. Morrison, H. Hoeck, J. Appl. Phys. 98 (2005) 093507.
[49] Y.C. Lin, C.L. Tseng, W.C. Chou, C.H. Chia, T.C. Han, J.L. Shen, J. Phys. Chem. C 115 (2011) 19962–19970.
[50] J.S. Reparaz, L.R. Muniz, M.R. Wagner, A.R. Goñi, M.I. Alonso, A. Hoffmann, B.K. Meyer, Appl. Phys. Lett. 96 (2010) 231906.
[51] J. Huso, J.L. Morrison, L. Bergman, M.D. McCluskey, Phys. Rev. B 87 (2013) 125205.
[52] W.L. Dang, Y.Q. Fu, J.K. Luo, A.J. Flewitt, W.I. Milne, Superlattices Microstruct. 42 (2007) 89–93.
[53] V. Gupta, A. Mansingh, J. Appl. Phys. 80 (1996) 1063–1073.
[54] J.L. Morrison, J. Huso, H. Hoeck, E. Casey, J. Mitchell, L. Bergman, M.G. Norton, J. Appl. Phys. 104 (2008) 123519.
[55] B.K. Meyer, H. Alves, D.M. Hofmann, W. Kriegseis, D. Forster, F. Bertram, J. Christen, A. Hoffmann, M. Straßburg, M. Dworzak, U. Haboeck, A.V. Rodina, Phys. Status Solidi B 241 (2004) 231–260.
[56] Roger H. French, J. Am. Ceram. Soc. 73 (3) (1990) 477–489.
[57] R.B. Laughlin, Phys. Rev. B 22 (1980) 3021–3029.